European Journal of Cell Biology 105 (2026) 151538

Contents lists available at ScienceDirect

European Journal of Cell Biology

journal homepage: www.elsevier.com/locate/ejcb

Human adipose stem cell conditioned medium has a pro-fibrotic and EMT-stimulating effect on urethral fibroblasts in vitro

Povilas Barasa [a,*], Emilija Baltrukonyte [a], Ieva Simoliune [a], Aivaras Grybas [b], Daiva Baltriukiene [a]

[a] Vilnius University, Life Sciences Center, Institute of Biochemistry, Vilnius, Lithuania
[b] Vilnius University Hospital Santaros Klinikos, Vilnius, Lithuania

ARTICLE INFO

Keywords:
Fibrosis
Myofibroblast
Secretome
Adipose stem cell
Conditioned medium

ABSTRACT

Fibrosis, characterized by excessive deposition of scar tissue, leads to the dysfunction of various organs. An urethral stricture, or pathological narrowing of the urethra, is an example of such scarring. The use of human adipose stem cell conditioned medium (HASC-CM) has shown promise as an anti-fibrotic treatment *in vivo*, as molecules produced by HASCs exhibit anti-inflammatory and fibrosis-modulating properties. However, HASC-CM has also been demonstrated to activate epithelial-to-mesenchymal transition (EMT) in cancer-associated cells. To elucidate whether HASC-CM promotes EMT or myofibroblast activation, we investigated its effects on primary human urethral fibroblasts (HUFs) and prostatic fibroblasts of the WPMY-1 line. We showed that HASC-CM promotes migration speed in HUFs but not in WPMY-1 cells while also increasing vimentin levels in the cells, both markers of EMT. Moreover, HASC-CM suppressed SMAD5 signalling in HUFs without altering SMAD3 signalling in either cell type. In addition, HASC-CM treatment induced myocardin-related transcription factor A (MRTF-A) nuclear translocation and increased amount of alpha smooth muscle actin (αSMA) in HUFs, indicating a shift towards the myofibroblast phenotype. We conclude that the effect of HASC-CM on WPMY-1 cells is negligible, however, this type of treatment has a pro-fibrotic and EMT-stimulating effect on HUFs.

1. Introduction

Tissue scarring remains a serious and still unsolved problem in modern medicine. Traumas, surgeries and other internal or external factors affecting tissues initiate the scarring process, which alters the architecture of organs and disrupts their function (Distler et al., 2019). The excessive deposition of scar tissue, rich in type I collagen and alpha smooth muscle actin (αSMA)-positive myofibroblasts defines the progression of fibrosis (Darby et al., 2014). This process is observed in the heart muscle after myocardial infarction, in the lungs after COVID-19 (Bari et al., 2021; Francis Stuart et al., 2016), or in the damaged urethra after trauma, surgery, or improper catheterization (Hirano et al., 2023). Due to fibrosis, the lumen of the urethra narrows, what causes serious urination difficulties and even urine retention with all its possible consequences. Urethral strictures are treated by incision of the scar, known as internal urethrotomy, dilation of the strictured site, or complete scar excision and primary anastomosis (Mangera and Chapple, 2010). Unfortunately, none of these methods are ideal because of frequent stricture recurrence. Internal urethrotomy can offer an overall stricture free rate of approximately 55% in short, soft strictures (Hillary et al., 2014). It has been noted that suppression of the fibrosis process could improve stricture treatment outcomes.

The main drivers of fibrosis are the proinflammatory activity of IL-1 cytokines (Borthwick, 2016) and the transforming growth factor beta (TGF-β)-dependent transformation of various cell types within the affected tissues (Hinz, 2015a). Normal cells undergo epithelial-to-mesenchymal transition (EMT) and subsequently acquire the myofibroblast phenotype (Feng et al., 2020). TGF-β is present in a latent form in the extracellular matrix (ECM) and is first released during tissue injury (Hinz, 2015b), and later during scar tissue formation, as a result of changes in ECM stiffness (Pang et al., 2017). As the scar tissue grows, this leads to a positive feedback loop of myofibroblast activation, which do not revert to their previous state. The persistent activation of myofibroblasts has been linked to prolonged stimulation through the TGF-β-SMAD signalling pathways (Finnson et al., 2020), and current treatment with TGF-β signalling inhibitors, such as pirfenidone, prevents

* Corresponding author.
E-mail address: povilas.barasa@gmc.vu.lt (P. Barasa).

https://doi.org/10.1016/j.ejcb.2026.151538
Received 4 November 2025; Received in revised form 7 April 2026; Accepted 8 April 2026
Available online 15 April 2026

the activation of new myofibroblasts and the deposition of new collagen fibrils (Lehtonen et al., 2016; Knuppel et al., 2017). In addition, inhibition of MRTF-A signalling in mechanosensitive fibroblasts has also been suggested as a treatment for fibrosis (Ma et al., 2023).

Human adipose stem cell conditioned medium (HASC-CM), rich in cytokines, chemokines and extracellular matrix molecules (Niada et al., 2021), has been demonstrated to have anti-inflammatory properties (Yano et al., 2022). Based on these findings, the application of HASC-CM or its components has also been proposed as a treatment of fibrosis, as they could modulate the activity of TGF-β and IL-1β-secreting macrophages at the site of injury (Bhattacharya and Ramachandran, 2023; Kruger et al., 2018). Importantly, it has shown anti-fibrotic effects in *in vitro* models of muscle and skin fibrosis (Yuan et al., 2017; Oki et al., 2021). However, HASC-CM has also shown epithelial-to-mesenchymal transition (EMT) promoting effects, which could have harmful consequences – such as stimulating the migration and tumorigenicity of the affected cells, as well as serving as a gateway to myofibroblast activation – if used as a treatment for humans (Iser et al., 2016; El-Hattab et al., 2020; Fabregat et al., 2016). Whether and how these effects are linked intracellularly has so far been unknown.

In this study, we aimed to investigate the potential link between the pro-EMT and fibrosis modulating properties of HASC-CM by analysing SMAD and MRTF-A signalling pathways in affected cells. To elucidate the effect of HASC-CM on different types of fibroblasts, we treated freshly isolated primary human urethral fibroblasts (HUFs) and prostatic fibroblasts of the WPMY-1 line with HASC-CM and analysed the expression of EMT and fibrosis markers, as well as the activation of the key intracellular signal transducers SMAD3, SMAD5 and MRTF-A.

2. Methods

2.1. Cell isolation

Human tissue samples for cell isolation were collected with the authorisation of the Lithuanian Bioethics Committee after the patients had signed an informed consent form. The urethral tissue samples were collected from male donors between 18 and 65 years of age. The procedures were approved by the Vilnius Regional Biomedical Research Ethics Committee: No. 2021/01–1297–775 and No. 158200–18/6–1044–544.

2.1.1. From adipose tissue

The adipose tissue samples for the isolation of human adipose tissue-derived stem cells (HASC) were taken from male perineal adipose tissue during urethral reconstructive surgery. For transportation, the samples were placed in Dulbecco's Modified Eagle Medium (DMEM; Gibco) with a 3-fold concentration of antibiotics (300 U/mL penicillin and 300 μg/mL streptomycin (Gibco)). The tissue was processed as follows: first it was washed in Hanks' Buffered Saline Solution (HBSS; Gibco) (without calcium or magnesium) for 10 min, then it was transferred to a tube containing trypsin-EDTA (Gibco) solution and mechanically dissociated; the tube was incubated for 60 min at 37°C in a thermomixer (Thermomixer Comfort, Eppendorf) with shaking at 300 rpm; the dissociating sample was pipetted thoroughly and then incubated for a further 30 min at 37°C before being centrifuged at 300 g for 10 min. The tissue pellet was resuspended in culture medium (see Section 2.3) and seeded into a 12-well plate.

2.1.2. From urethral tissue

Urethral tissue samples were taken from the bulbar part of the male urethra when reconstructive urethral surgery was performed. After dissection of the strictured urethra, fibrotic tissue was harvested for isolation of human urethral fibroblasts (HUF). The sample sites were examined histologically to confirm the quality of the fibrotic urethral biopsies. The samples were transported in parallel to the adipose tissue samples. The tissue was first washed with HBSS (with calcium and magnesium, Gibco) for 10 min, then transferred to a tube containing type I collagenase (Gibco) and mechanically dissociated. The tube was incubated for 2 h at 37°C with shaking at 300 rpm. After dissociation, the sample was centrifuged at 300 g for 10 min. The resulting pellet was resuspended in a culture medium (see Section 2.3) and seeded in a 12-well plate.

2.2. Coating of the culture surface for fibroblast and myofibroblast cells

The surfaces used for the cultivation of HUF and WPMY-1 cells and the experiments were coated as follows: first, a solution of Sylgard 184 (Dow) was prepared by thoroughly mixing Sylgard base with Sylgard crosslinker at a ratio of 40:1; the solution was deaerated by keeping it under vacuum for about 10 min until all bubbles had disappeared. The solution was then poured into plates, chamber slides or flasks and incubated at 37°C for 24 h. The surfaces were then washed with phosphate-buffered saline (PBS; Gibco) and coated with fibronectin at 2 $\mu g/cm^2$.

2.3. Cell cultivation

All cells were maintained in a humidified 37°C incubator with 5% CO_2 (Thermo Fisher Scientific). HASC were maintained in Iscove's modified Dulbecco's medium (IMDM; Gibco) containing 10% foetal bovine serum (FBS; Gibco), 100 U/mL penicillin (Gibco), 100 μg/mL streptomycin (Gibco) and 1% GlutaMAX (Gibco). WPMY-1 (ATCC, CRL-2854), the human prostate cancer stromal myofibroblast cell line, was maintained in DMEM with 5% FBS, 100 U/mL penicillin, 100 μg/mL streptomycin and 1% GlutaMAX supplement (Gibco). HUF were grown in DMEM with 20% FBS (Gibco), 100 U/mL penicillin-100 μg/mL streptomycin and 1% GlutaMAX supplement. Primary cells from passages 4–9 were used for the experiments, while WPMY-1 were used up to passage 15.

2.4. Flow cytometry

The isolated HASC monolayer was dispersed with 1 mM ethylenediaminetetraacetic acid (EDTA; Thermo Fisher Scientific) in PBS, and 3×10^5 cells/mL were used for each surface marker analysis. Cells were washed twice with 3% bovine serum albumin (BSA; Invitrogen) in PBS and then incubated with primary antibodies against: CD44 (1:1000; MA5–12394; Invitrogen), CD45 (0.5:1000; 14–0459–82; Invitrogen) and CD90 (1:1000; 14–0909–82; Invitrogen) for 30 min at 4 °C. Cells were washed twice with 3% BSA in PBS and then incubated with an R-phycoerythrin-conjugated secondary antibody (1:1000; P852; Invitrogen) diluted in 3% BSA prepared in PBS at 4 °C for 30 min. The cells were then washed twice, suspended in ice-cold PBS and analysed using the BD FACSCanto™ II system (BD Biosciences) measuring at least 1×10^4 events. To determine background fluorescence, HASC were labelled with anti-mouse IgG1 isotype controls (1:100; MA5–18092; Invitrogen). Data were analysed using the Flowing software (version 2.5.1; Turku Bioscience).

2.5. Evaluation of adipose cell stemness

HASC were chemically stimulated to differentiate into three cell types using the following media: for myogenic differentiation - low glucose DMEM (Gibco) supplemented with 2% horse serum (Gibco); for adipogenic differentiation – high glucose DMEM supplemented with 10 μg/mL insulin, 1 μM dexamethasone (Sigma-Aldrich), 10 μM indomethacin, 500 μM IBMX and 10% FBS; for osteogenic differentiation – IMDM supplemented with 1 mM β -glycerophosphate (Sigma-Aldrich), 10 nM dexamethasone, 50 μg/mL ascorbic acid (Sigma-Aldrich) and 10% FBS. The regular cell culture medium was replaced with the aforementioned media and the cells were cultured for 7 days to allow induced differentiation to occur. Subsequently, the cells were washed

three times with PBS and stained for differentiation markers. To assess adipogenic differentiation, the cells were first fixed with 4% PFA (Roth) for 30 min at room temperature and then washed three times with PBS. The cells were then incubated with 60% isopropanol (Sigma-Aldrich) for 10 min and stained with Oil Red O (Sigma-Aldrich) dissolved in 60% isopropanol for 10 min. The cells were then washed three times with distilled water and imaged under a light microscope. To assess myogenic differentiation, cells were stained for 5 min with a 0.1% crystal violet solution (Sigma-Aldrich) in 20% ethanol (Vilniaus Degtine), then washed three times with PBS and imaged. To assess osteogenic differentiation, the cells were stained for 10 min with a filtered 2% Alizarin S (Sigma-Aldrich) solution. The cells were then washed three times with PBS and imaged.

2.6. Preparation of the conditioned medium from human adipose-derived stem cells (HASC-CM)

HASC-CM was prepared as follows: the HASC cell monolayer was dispersed and the cells were seeded in T75 tissue culture flasks (TPP) in culture medium (DMEM supplemented with 10% FBS and 100 U/mL penicillin-100 µg/mL streptomycin) at a density of 7000 cells/cm^2. After 24 h, the HASC-conditioned medium (HASC-CM) was collected and immediately used for experiments.

2.7. Scratch assay

HUF and WPMY-1 cells were seeded into 34 mm diameter cell culture dishes (TPP) with Ibidi inserts (80469, Ibidi GmbH, Gräfelfing, Germany) at a density of 3×10^5 cells/mL to obtain a confluent cell layer. 110 µl of the cell suspension was added directly to each well. After seeding, the cells were grown for 24 h until they reached confluence. After incubation, the inserts were carefully removed with sterile tweezers to create a cell-free area ("scratch") approximately 500 µm width. The cells were then washed once with PBS to remove cell debris and non-adherent cells. 1 mL of DMEM with 10% FBS or HASC-CM. At different time intervals, fields of the scratch area horizontally were visualized using a microscope (Olympus IX51) at 4x magnification. Images were taken at 0 h to capture the initial area of the scratch, and recovery of the monolayers was assessed after 3, 6, 16, 20 and 24 h. All measurements of the different treatments were performed by analysing four different fields of scratch area per sample. In total, 5 samples from each treatment at each time point were used. The scratch area at the selected time points was calculated by measuring the remaining cell-free area using ImageJ software.

2.8. MTT assay

HUF cells were seeded into 12-well plates at a density of 1×10^4 cells/well and incubated overnight. The cultures were then left untreated (by refreshing the culture medium) or treated with HASC-CM for 24 h. Afterwards, the media were removed, the cultures washed once with PBS and incubated with 0.5 mg/mL MTT (Roth) solution in PBS for 1 h in 37°C. The solution was then removed and the formazan crystals dissolved in 500 µl DMSO for 5 mins with gentle shaking. 200 µl of the samples were transferred into a 96-well plate. The 570 nm and 650 nm (background) absorbance in the wells was measured with Varioskan Flash Multimode Plate Reader (Thermo Fisher).

2.9. Immunocytochemistry

HUF and WPMY-1 cells were seeded at a density of 1×10^4 cells/cm^2. After 1 day of cultivation, the medium was removed and the cells were left untreated (medium replaced with DMEM containing 10% FBS), treated with HASC-CM, 10 ng/mL TGFβ or HASC-CM with 10 ng/mL TGFβ. After 24 h, the samples were washed with PBS and fixed with 4% PFA for 15 min. Then the samples were washed three times with PBS and placed in PBST permeabilization solution (0.3% Tween 20 (Sigma-Aldrich) in PBS) for 30 min. Samples were blocked for 2 h with 1% BSA, 10% goat serum (Sigma-Aldrich) and 0.3 M glycine (Roth) solution in PBST and then washed again three times. The samples were incubated with the primary antibodies in the blocking solution overnight at 4°C. The samples were then washed again and incubated with AlexaFluor 488-conjugated or AlexaFluor 594-conjugated secondary antibodies (Thermo Fisher) for 1 h at RT. After washing in PBS to remove unbound antibodies, samples were treated with 1 µg/mL DAPI (Invitrogen) for 15 min, washed three times with PBS and fixed with Mowiol (Roth). Samples were observed and photographed using a confocal microscope (Leica). To evaluate the subcellular localization of MRTF-A, the mean fluorescence intensity of labelled MRTF-A in the nuclei (counterstained with DAPI) and surrounding cytoplasm was quantified using ImageJ software. Cells with higher mean nuclear fluorescence were considered MRTF-A nuclear-dominant. For this analysis, a total of 6 images per experimental group were used and all cells fully visible in the image included in the analysis (average of 15 cells per image).

For a full list of primary and secondary antibodies used, refer to Supplementary Table S2.

2.10. Immunoblotting

Cells were seeded in 6-well plates at a density of 2×10^5 cells/well. After 1 day of cultivation, the medium was removed and the cells were left, treated with HASC-CM, 10 ng/mL TGFβ or HASC-CM with 10 ng/mL TGFβ. 24 h later, the cells were washed twice with PBS and frozen at −20°C. Scrapers and RIPA lysis buffer (25 mM Tris HCl (Carl Roth), 150 mM NaCl (Carl Roth), 1% Triton-X (Sigma-Aldrich), 1% sodium deoxycholate, 0.1% SDS, 1 mM PMSF (Thermo Scientific), 1 mM sodium orthovanadate (Carl Roth) and 10 µg/mL aprotinin (Thermo Scientific)) were used to extract the proteins. Protein concentration was determined using the Micro BCA kit (Thermo Fisher) according to the manufacturer's instructions. The sample concentration was equalized with RIPA buffer, 4x protein sample buffer (10 mM Tris Base, 40% glycerol, 8% SDS, 0.001% bromophenol blue (Sigma-Aldrich) and 4% mercaptoethanol (Sigma-Aldrich)) was added and the samples were heated at 95°C for 5 min. The prepared samples were stored at −20°C until analysed. Proteins were separated by SDS-PAGE and transferred to a nitrocellulose membrane (Amersham) by wet transfer (for ROCK1 and ROCK2 proteins) overnight or by semi-dry transfer for 25–50 min (depending on the molecular weight of the protein analysed). The membranes were briefly washed with deionised water and blocked for 1 h with ROTI-block (Carl Roth) in TBST. They were then incubated overnight at + 4°C with primary antibodies (anti-GAPDH, SDHA, ROCK1, ROCK2, RhoA, SMAD5, phospho-SMAD5, SMAD3, phospho-SMAD3, αSMA (Thermo Fisher)) in blocking solution. They were then washed three times for 5 min with TBST, secondary antibodies (HRP-conjugated anti-mouse or anti-rabbit antibodies, Carl Roth) were applied for 1 h in RT and then washed three times. Pierce ECL Western Blotting Substrate (Thermo Fisher) was used for chemiluminescence. A UVITEC device (UVITEC Cambridge) was used for visualisation, and images were analysed using ImageJ version 1.52a. For a full list of antibodies used in the immunoblotting experiments, see Supplementary Table S2.

2.11. Quantitative PCR

Cells were seeded in 6-well plates at a density of 2×10^5 cells/well. After 1 day of cultivation, the medium was removed and the cells were left untreated, treated with HASC-CM, 10 ng/mL TGFβ or HASC-CM with 10 ng/mL TGFβ. After 24 h, the samples were washed twice with PBS. Trizol (Thermo Fisher) was used for RNA isolation according to the manufacturer's instructions. RNA electrophoresis was performed to evaluate the quality and quantity of the isolated RNA. The Maxima H Minus First Strand cDNA Synthesis Kit with dsDNAse (Thermo Fisher) was used to synthesise cDNA according to the manufacturer's

instructions. The Luminaris Colour HiGreen qPCR Master Mix (Thermo Fisher) was used to perform quantitative PCR according to the protocol provided. The results were analysed manually and the relative gene expression values were quantified using *GAPDH* as a reference gene. Primer sequences for qPCR were obtained from PrimerBank and are listed in SupplementaryTable S1. To investigate the effect of HASC-CM on the expression of components of TGFβ, TaqMan Array Human TGFB Pathway (Thermo Fisher) plates were used. The qPCR mix for these reactions was the TaqMan Gene Expression Master Mix (Thermo Fisher). The reference genes for this analysis were *GAPDH, 18S, HPRT1* and *GUSB*.

2.12. Cytokine detection array

The partial characterization of HASC-CM contents was completed using the Proteome Profiler Human XL Cytokine Array Kit (R&D Systems). The assay was performed according to the manufacturer's instructions. Briefly, the dot-blot membranes were blocked using the provided blocking solution. Regular culture medium was prepared and HASC-CM was collected, mixed with the assay buffer and incubated on the membranes overnight in + 4°C. The antibody cocktail was applied, followed by incubation in the ECL solution, and the chemiluminescence was detected using the UVITEC device. The signal strength of analyzed proteins was calculated as a ratio between the luminescence in the HASC-CM samples and regular culture medium sample.

2.13. Statistical analysis

The statistical analysis was performed, and graphs were created using R software (version 4.2.2). Outliers of the TaqMan Array gene expression analysis' results were removed prior to calculations using the interquartile range (IQR) method. The Shapiro-Wilk test was used to determine whether the data were normally distributed. The two-tailed Welch test was used when two experimental groups were compared and the Tukey test was used when there were more than two groups, whereas Benjamini-Hochberg correction was used for the gene expression time-course analysis. One-tailed Welch test was used to determine the presence of cytokines in HASC-CM. The significance level α was chosen to be equal to 0.05. Significant differences are marked with symbols and are explained below the figures.

3. Results

In this study, we used primary human adipose stem cells (Supplementary Fig. 1, A), which were positive for CD44 (mean and SD equal to 46.26 ± 19.68%, N = 3) and CD90 (91.57 ± 11.7%, N = 3) (Supplementary Fig. 1, B) and demonstrated mesenchymal differentiation potential towards adipose, muscle and bone tissue (Supplementary Fig. 1, C). As fibroblasts have been shown to spontaneously transform into myofibroblasts during cultivation *in vitro* (Baranyi et al, n.d), we chose to use freshly isolated primary urethral fibroblasts and a fibroblast cell line (WPMY-1, originally described as a myofibroblast cell line due to co-expression of αSMA and vimentin (Webber et al., 1999)). Both cell types were cultured on FN-coated PDMS, to compare how HASC-CM could affect the different cells present in the urinary tract stroma in a biologically-relevant *in vitro* model of fibrosis progression. The PDMS substrate had a theoretical elasticity value E between ~36 and 54 kPa (Darby et al., 2022). The HUFs (Supplementary Fig. 1, D) used for the experiments were positive for αSMA (Supplementary Fig. 1, F) and vimentin (Supplementary Fig. 1, G). HUFs from different donors were used as biological replicates in the experiments. The WPMY-1 cells (Supplementary Fig. 1, E) had a higher amount of αSMA than HUFs (Supplementary Fig. 1, H) and were also positive for vimentin (Supplementary Fig. 1, I). Measuring the relative gene expression levels, we discovered several significant differences between WPMY-1 cells and HUFs (Supplementary Fig. 1, J): although under standard culture conditions WPMY-1 cells expressed less *CTGF,* which is an early fibrosis marker (Lipson et al., 2012), than HUFs, they expressed significantly more *PAI1* and *VEGFA*, both of which are markers for advanced fibrosis (Ghosh and Vaughan, 2012; Huang et al., 2023); and the ratio of *MMP1*:*TIMP1* relative expression was lower in WPMY-1 cells than HUFs (0.01 vs 0.113). The lower ratio of MMP1 (collagenase I) amount to TIMP1 (tissue inhibitor of metallproteases 1) amount has been observed in late stage urethral strictures (Prihadi et al., 2018). Comparing the two cell types, we can thus summarize that WPMY-1 cells, by virtue of abundant αSMA and their greater expression of the PAI-1 protease inhibitor gene *PAI1*, as well as lower ratio of *MMP1*:*TIMP1* expression, exhibit higher levels of myofibroblast markers under regular culture conditions *in vitro*.

3.1. The appearance of EMT markers in HUFs is stimulated by HASC-CM

The process of EMT can be analysed by measuring markers of mesenchymal cells, such as migration speed and the amount of vimentin protein (Usman et al., 2021). As the cells used in this study are already of mesenchymal origin, we hypothesized that HASC-CM could instead increase the amount or intensity of mesenchymal markers by altering the gene expression profile of the cells. We tested whether HASC-CM affects the migration speed of HUF and WPMY-1 cells using a scratch assay. The results obtained showed that HUF cells affected by HASC-CM expanded over the scratch area faster than untreated cells (Fig. 1, A). To confirm whether the closure occurred due to migration rather than cell proliferation, we conducted an MTT assay, which showed no significant difference in formazan absorption between untreated and HASC-CM-treated cells, suggesting there was no substantial change in cell number during the period of migration (Supplementary Fig. 2, A). Meanwhile, HASC-CM had no significant effect on the migration speed of WPMY-1 cells (Fig. 1, B). These results allowed us to infer that the actin polymerisation machinery – responsible for cellular migration – in HUFs is activated by HASC-CM. To further confirm whether HASC-CM induces EMT, we measured the levels of the cytoskeletal proteins fibrillar actin (or F-actin) and vimentin in HUFs and WPMY-1 cells treated with HASC-CM for 24 h. HUFs had significantly increased levels of both F-actin and vimentin 24 h after treatment with HASC-CM, while WPMY-1 cells showed no changes in F-actin levels but had increased levels of vimentin (Fig. 1, C).

3.2. HASC-CM suppresses SMAD5 signalling in HUFs

To determine the underlying gene expression changes HASC-CM induced by in HUFs, we treated the cells with HASC-CM and, after 24 h, measured changes in the gene expression of various components of the TGFβ signalling pathway (Fig. 1, D). We observed a statistically significant decrease in the expression of *HIPK2, RHOA, PAI1, ACVR2* and *MAPK1* genes. ACVR2 is part of the heteromeric receptor that phosphorylates SMAD3 upon activin binding; HIPK2 has been implicated as a co-activator of transcription with SMADs (Garufi et al., 2023); whereas *PAI1, RHOA* and *MAPK1* expression is activated by the phospho-SMAD5 transcription factor. Hence, we hypothesised that HASC-CM might attenuate SMAD5-driven transcription by reducing its phosphorylation. To elucidate what molecules of the HASC-CM could influence the dephosphorylation of SMAD5, we conducted a partial characterization of its protein components (Fig. 2). The analysis revealed the presence of a number of pro-inflammatory cytokines (IL-1a, IL-2, IL-6), which could stimulate the activity of PPM1A phosphatase, a known suppressor of SMAD1/5 signalling (Kokabu et al., 2012). We also detected the presence of the fibroblast chemotaxis stimulating chemokine CXCL12 (SDF-1) and PDGFB, which is known to facilitate MRTF-A-driven gene expression changes (Vasudevan and Soriano, 2014; Chen et al., 2024), both of which could explain the appearance of EMT markers.

Western blotting experiments showed that HASC-CM indeed statistically significantly reduced the phosphorylation of SMAD5 in HUFs 24 h after treatment. However, when HUFs were additionally stimulated

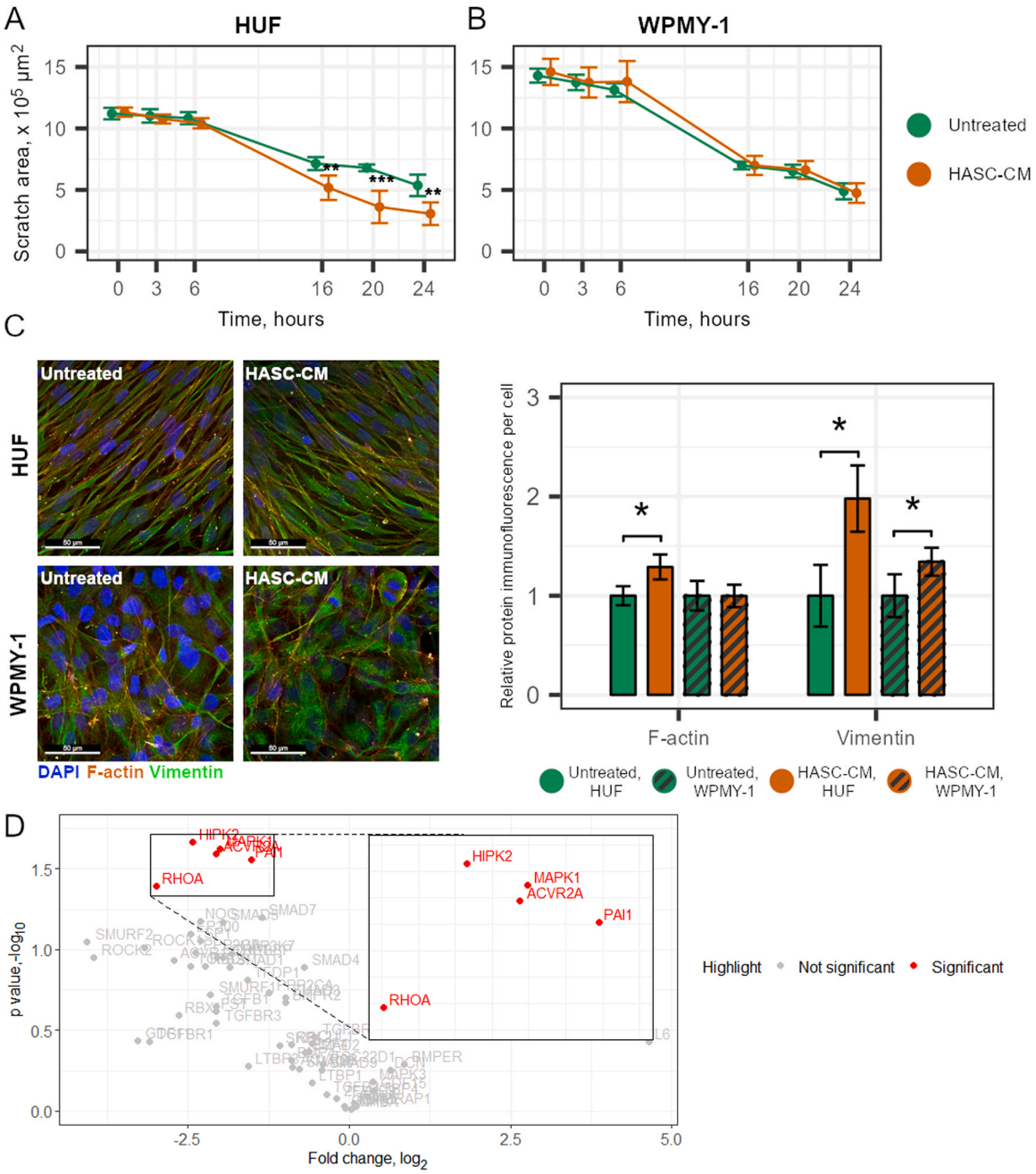

Fig. 1. Results of the scratch assay of HUFs (A) and WPMY-1 (B), untreated or treated with HASC-CM. N = 5. Mean values (dots) and SD (bars) are shown. (C) Immunofluorescence of F-actin (TRITC-phalloidin labelling, orange) and vimentin (AlexaFluor 488 labelling, green) calculated for untreated and HASC-CM-treated HUF and WPMY-1 cells. The cell nuclei were stained blue with DAPI. N = 3 (HUF) and 5 (WPMY-1). (D) Relative gene expression changes between untreated and HASC-CM-treated HUFs. Genes with statistically significant ($p < 0.05$) altered gene expression levels are highlighted in red. N = 3-4. Stars denote statistically significant (* - $p < 0.05$, ** - $p < 0.01$, *** - $p < 0.001$) differences between the groups.

with TGFβ, the effect disappeared (Fig. 3, A). Because *RHOA* encodes the RhoA protein, essential in the Rho-ROCK signalling pathway (which modulates actin polymerization), we performed Western blotting to determine whether the components of this pathway are affected by HASC-CM. The analysis suggested no change in the amount of RhoA, ROCK1 or ROCK2 (Supplementary Fig. 2, B) after 24 h of treatment with HASC-CM. In WPMY-1 cells, HASC-CM did not suppress SMAD5 phosphorylation with or without concurrent TGFβ treatment (Fig. 3, B). Interestingly, HASC-CM did not suppress SMAD3 signalling at the same time point in either cell type (Supplementary Fig. 2, C).

3.3. *HASC-CM stimulates MRTF nuclear translocation in HUFs, leading to EMT and fibrosis-related gene expression changes*

To link the observed changes in SMAD5 signalling and cytoskeletal dynamics, we proceeded to investigate whether the activity of MRTF-A transcription factor in HUFs or WPMY-1 cells is altered by HASC-CM treatment. Loss of SMAD5 has been linked to increased migration rate and alterations of actin polymerization dynamics in stromal cells (Allaire et al., 2011). Meanwhile, the relative increase in the amount of F-actin could lead to nuclear translocation of MRTF-A, which, in turn, could trigger far-reaching changes in EMT and fibrosis-related gene expression (Gau and Roy, 2018). When calculating the proportion of

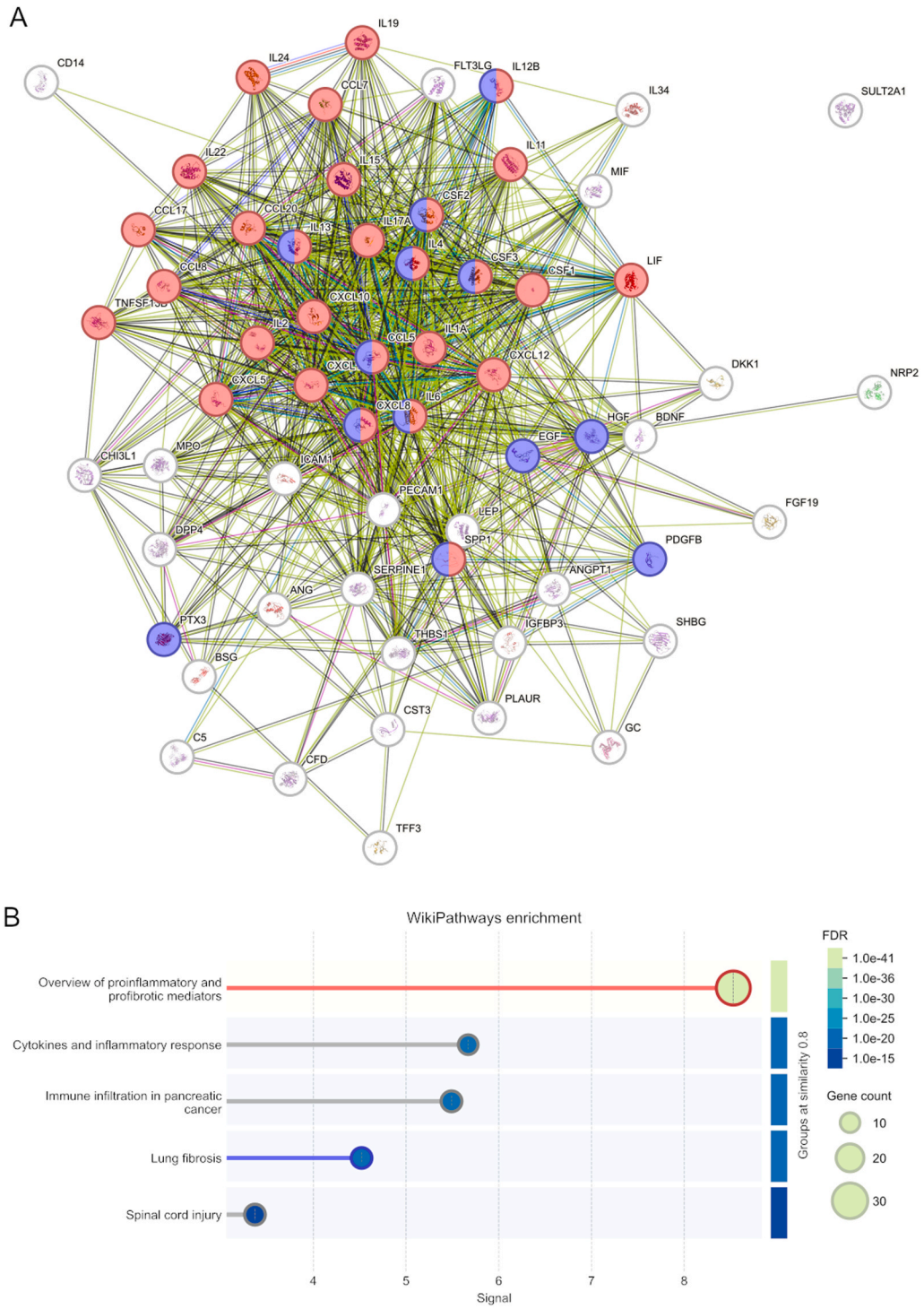

Fig. 2. Analysis of HASC-CM cytokine content. Proteins were detected using a dot-blot array, and the presence of specific cytokines was confirmed by calculating the signal ratio between HASC-CM and regular culture medium. A – graph of STRING database functional interactions between the identified components of HASC-CM. B – the top 5 annotated signalling pathways with the highest enrichment scores. The colour scale (blue-green) denotes the false discovery rate (FDR), describing how significant (in p-value) the enrichment is. X axis (signal) shows harmonic mean between the observed enrichment/expected enrichment ratio and -log(FDR). Proteins annotated as belonging to the "Overview of proinflammatory and profibrotic mediators" pathway highlighted in red, and those belonging to "Lung fibrosis" pathway highlighted in blue.

cells with nuclear-dominated MRTF-A (as opposed to cytoplasmic-dominated MRTF-A), we found that there are significantly more cells with nuclear-localized MRTF-A when the HUFs are stimulated with HASC-CM for 24 h (Fig. 3, C). However, this effect disappeared upon stimulation with TGFβ, suggesting that the increased phosphorylation of SMAD5 or SMAD3 attenuates the nuclear translocation of MRTF-A. Meanwhile, the subcellular location of MRTF-A in WPMY-1 cells was not affected by stimulation with either HASC-CM and/or TGFβ (Fig. 3, D). Under all conditions tested, MRTF-A was predominantly localised in the nucleus in WPMY-1 cells. To confirm whether the nuclear translocation of MRTF-A could lead to changes in EMT-related and fibrosis-related gene expression, we measured the relative amount

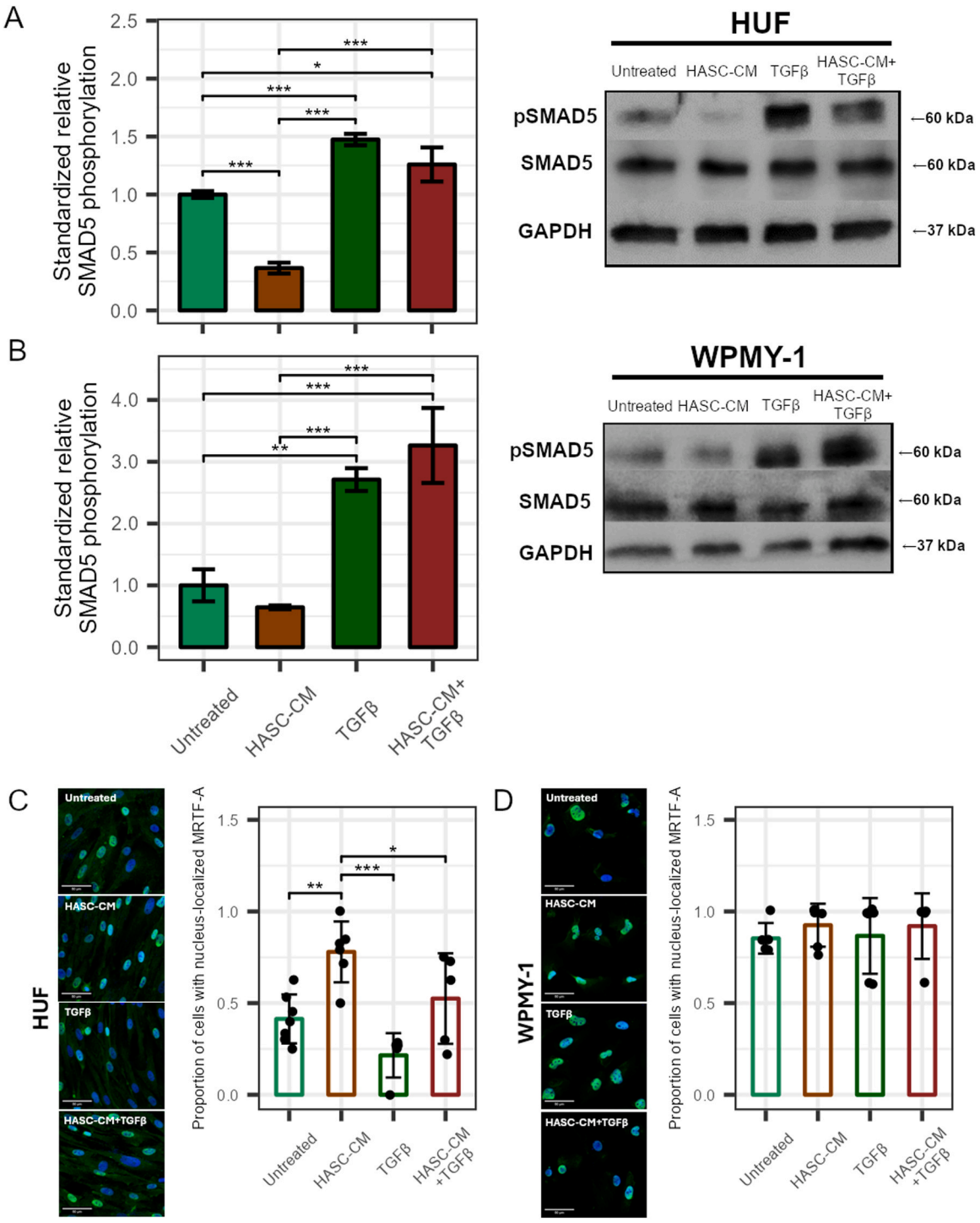

Fig. 3. SMAD5 phosphorylation in HUF (A) and WPMY-1 cells (B) that were untreated, treated with HASC-CM, 10 ng/mL TGFβ or both. Means (columns) and SD (bars) are displayed. N = 3. Stars denote statistically significant (* - $p < 0.05$, ** - $p < 0.01$, *** - $p < 0.001$) differences between the groups. Immunocytochemical measurement of translocation of MRTF-A (AlexaFluor 488 labelling, green) in HUF cells (C) and WPMY-1 cells (D) that were untreated, treated with HASC-CM, 10 ng/mL TGFβ or both. N = 6. The scale bars represent 50 μm. Mean values (columns), data points (dots) and SD (bars) are shown. The cell nuclei were stained blue with DAPI. Stars denote statistically significant (* - $p < 0.05$, ** - $p < 0.01$, *** - $p < 0.001$) differences between the groups.

of transcripts for *SNAIL1, SNAIL2,* which encode mesenchymal cell transcription factors (Sobierajska et al., 2020), *TWIST1*, coding for an oncogene linked to fibroblast activation (García-Palmero et al., 2016), and the genes *COL1A1, COL3A1* and *ACTA2*, which encode type I and III collagens and smooth muscle actin, markers of myofibroblast activation. Comparing the results of the cell types side by side, HASC-CM increased the expression of both *SNAIL1* and *SNAIL2* in HUFs (Fig. 4, A, B), but not in WPMY-1 (Fig. 4, G, H). Moreover, the effect of TGFβ on HUFs significantly decreased the expression of *TWIST1*, regardless of parallel treatment with HASC-CM (Fig. 4, C); had a tendency to increase the expression of *COL1A1* (Fig. 4, E); and strongly upregulated the expression of *ACTA2* (Fig. 4, D). Interestingly, the expression of *ACTA2* was significantly more increased in HUFs treated with a combination of HASC-CM and TGFβ compared to TGFβ alone. All of the aforementioned

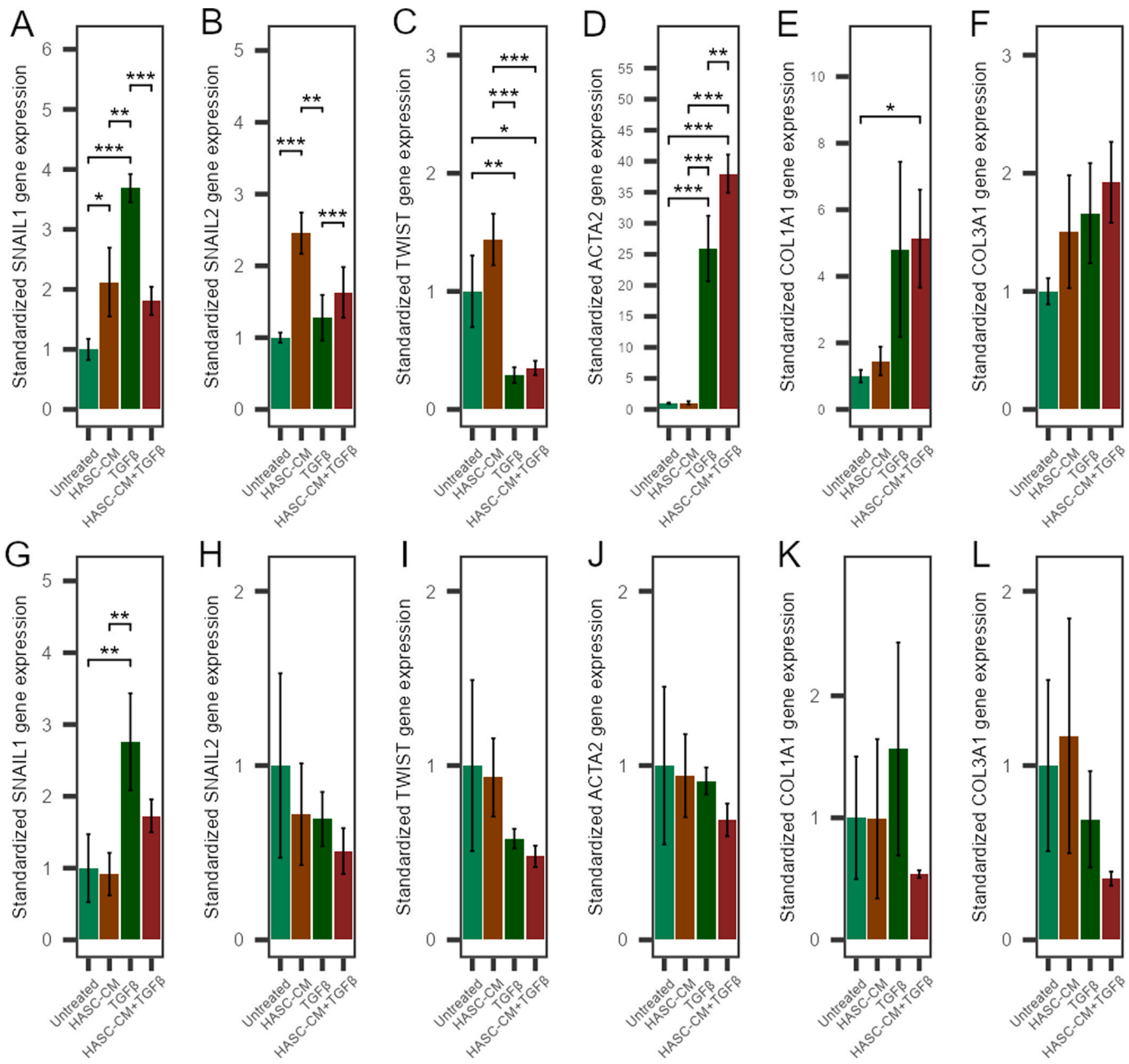

Fig. 4. HASC-CM stimulates EMT-related gene expression in HUF cells. HUF (A-F) and WPMY-1 (G-L) were left untreated, treated with HASC-CM, 10 ng/mL TGFβ or both. Relative *SNAIL1* (A, G), *SNAIL2* (B, H), *TWIST* (C, I), *ACTA2* (D, J), *COL1A1* (E, K) and *COL3A1* (F, L) gene expression levels, normalised to *GAPDH* expression, were analysed. N = 3. Mean values (columns) and SD (bars) are shown. Stars denote statistically significant (* - $p < 0.05$, ** - $p < 0.01$, *** - $p < 0.001$) differences between the groups.

effects were absent when WPMY-1 were treated with HASC-CM, TGFβ, or a combination of both. Only the expression of *SNAIL1* was significantly increased in WPMY-1 when treated with TGFβ compared to untreated cells (Fig. 4, G).

3.4. HUFs treated with HASC-CM contain higher amount of αSMA

As our gene expression analysis showed that HASC-CM in combination with TGFβ treatment induced greater expression of *ACTA2* in HUFs compared to TGFβ treatment alone, we investigated whether HASC-CM treatment could lead to increase of αSMA in the affected cells. Surprisingly, all chosen treatments increased the amount of this myofibroblast marker in HUFs (Fig. 5, A), but not in WPMY-1 cells (Fig. 5, B). To more precisely determine the dynamics of *ACTA2* expression in HASC-CM stimulated HUFs, we measured the transcript levels at 3, 6, 12 and 24 h after treatment (Supplementary Fig. 3). There was a significant relative increase in *ACTA2* expression in HASC-CM-treated HUFs at the 3 and 12 h time points.

4. Discussion

The natural environment of fibroblasts contains a plethora of extracellular matrix proteins, which provide structural support and facilitate intercellular communication. The signals that fibroblasts receive from their *in vitro* environment come from their culture medium. The most common *in vitro* culture methods use foetal bovine serum in the liquid culture media to supply some of the extracellular signals necessary for fibroblast survival and proliferation (Lee et al., 2022). Recently, alternatives to foetal bovine serum, such as human platelet lysate, have been investigated for the cultivation of human

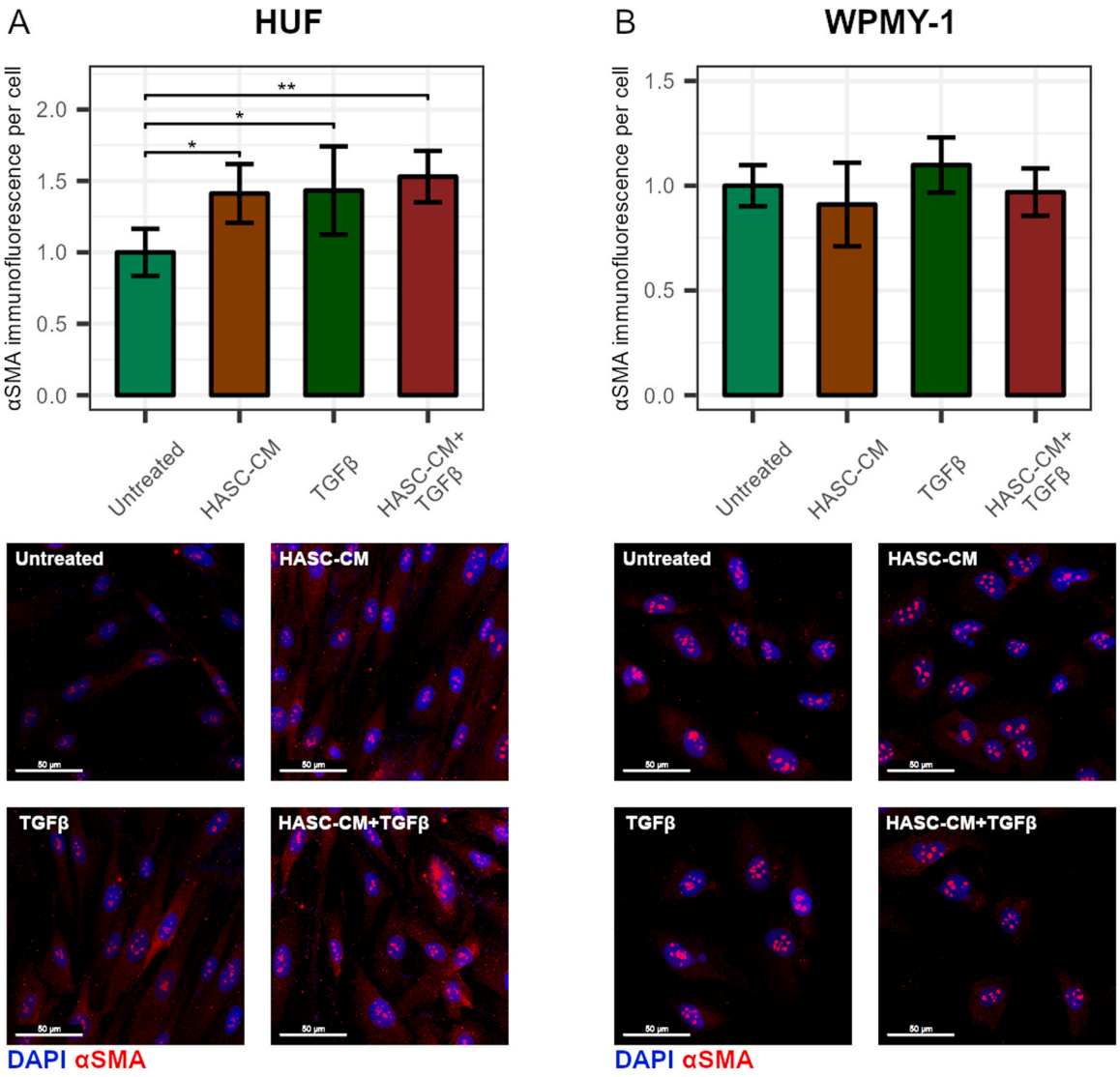

Fig. 5. Immunofluorescence results measuring the amount of αSMA in HUF (A) and WPMY-1 (B) cells that were untreated, treated with HASC-CM, 10 ng/mL TGFβ or both. N = 3. Mean values (columns) and SD (bars) are shown. Stars denote statistically significant (* - $p < 0.05$, ** - $p < 0.01$, *** - $p < 0.001$) differences between the groups. Representative images of αSMA (AlexaFluor 594, labelled red) and cell nuclei staining (blue, with DAPI) provided. The scale bars represent 50 μm.

mesenchymal cells (Du et al., 2022). The switch into serum-free media, as performed in some studies, induces cellular stress, stimulates autophagic flux, and may cause fibroblast transformation into myofibroblasts (Lehrich et al., 2021; Galie et al., 2011). The culture medium can be pre-conditioned by other cells, such as the HASCs used in our study. Identification of the specific components of HASC-CM can be complicated by the presence of serum, however, methods have been developed to distinguish cell products from serum components present in the same medium (Lehrich et al., 2021; Nakamura et al., 2021; Shin et al., 2019). Similar to other studies (Kruger et al., 2018; Iser et al., 2016; El-Hattab et al., 2020), the HASC-CM contains various factors secreted into the medium by HASCs which have been themselves cultivated in regular, serum-containing culture medium.

The components of the mesenchymal stem cell (MSC) secretome have been investigated for the treatment of various inflammatory and fibrotic diseases (Bari et al., 2021; Choi et al., 2024a, 2024b; Harrell et al., 2019; Basalova et al., 2020; Filidou et al., 2022), suggesting positive outcomes *in vivo*. HASCs, a type of MSC (Bacakova et al., 2018), have also been explored for their use in regenerative medicine, including cell-free therapy, where molecules produced by HASCs would be utilized (Trzyna and Banaś-Ząbczyk, 2021a). Partial characterization of the protein content of HASC-CM used in our study revealed a variety of anti-inflammatory (IL-4, IL-19) and pro-inflammatory cytokines (IL-1a, IL-2, IL-6), a soluble interleukin receptor (ST2) and growth factors (PDGF, HGF, EGF) which have also been identified in other analyses of the HASC secretome (Trzyna and Banaś-Ząbczyk, 2021b). Notably, IL-1a and ST2 have been noted for their role in stimulating fibrosis (Borthwick, 2016). Due to the high complexity of the stem cell secretome (Kehl et al., 2019), it is natural that pleiotropic effects of HASC-CM on fibroblasts can be observed. Our data show that HASC-CM stimulates the appearance of cellular markers of EMT: it increases the migration speed of HUF cells and the amount of vimentin protein in both HUF and WPMY-1 cells, which is consistent with the results of a study using C6 glioma cells (Iser et al., 2016). The observed increase in F-actin was also found in MSC-CM-treated hepatoma cells (Li et al., 2015).

To understand the underlying cause of these changes, we investigated the effect of HASC-CM on TGFβ signalling. TGFβ is considered to be one of the most important cytokines triggering tissue fibrosis, as it is produced by both immune cells arriving at the site of tissue injury and by myofibroblasts themselves (Meng et al., 2016; Chung et al., 2021). TGFβ binding to its receptors has been shown to stimulate both EMT and the transformation of fibroblasts, however, the role of

TGFβRII→ALK1→SMAD1/5-mediated signalling in fibrosis has often been overshadowed by the importance of related TGFβRII-→ALK5→SMAD2/3-mediated signalling (Muñoz-Félix et al., 2013). Our experiments have shown that HASC-CM has no suppressive effect on SMAD3 signalling, similar to studies with human dermal fibroblasts (El-Hattab et al., 2020; Li et al., 2019). SMAD5 has recently been shown to play an important role in regulating actin cytoskeleton polymerisation, associated EMT processes and fibrosis progression (Allaire et al., 2011; Curado et al., 2014; Latha et al., 2021). Our data show that SMAD5 signalling in HUFs is suppressed by HASC-CM-induced dephosphorylation of SMAD5, as well as the downregulation of the expression of SMAD5-regulated genes *MAPK1*, *ACVR2A* and *PAI1*, whereas no such dephosphorylation occurs in WPMY-1.

The dynamics of actin polymerisation generate the forces that drive cellular movement (Schaks et al., 2019), and we have shown that HASC-CM activates the polymerisation of G-actin into F-actin in HUFs. The observed changes in actin polymerisation are thought to be driven by ROCK1/2→LIMK→cofilin signalling (Lee et al., 2019), and activated SMAD5 may modulate this process by controlling cofilin phosphorylation (Allaire et al., 2011), linking the observed dephosphorylation of SMAD5 to the increase in F-actin levels. MRTF-A is translocated to the nucleus when G-actin polymerises into F-actin (Miranda et al., 2021). This transcription factor, together with its transcriptional cofactor SMAD3, is known to stimulate the expression of the mesenchymal transcription factor genes *SNAIL1* and *SNAIL2* (Miranda et al., 2021). Specifically, in the context of fibrosis, MRTF-A has been shown to modulate the expression of such EMT-related genes (Sobierajska et al., 2020). Moreover, MRTF-A, in complexes with serum response factor (SRF) – another transcription cofactor – is similarly known to promote the expression of *SNAIL1* and *SNAIL2 (*Gau and Roy, 2018*)*. We showed that HASC-CM increases the amount of MRTF-A localised in the nuclei, which is caused to the observed increase of F-actin in HUFs. In contrast, in WPMY-1, HASC-CM did not stimulate an increase in the amount of F-actin, and the localisation of MRTF-A within these cells remained unchanged regardless of treatment. Our results are consistent with the established mechanisms and provide the link between HASC-CM-induced SMAD5 dephosphorylation, MRTF-A nuclear translocation and MRTF-A-SMAD3- and MRTF-A-SRF-mediated expression of EMT genes in fibroblasts (Fig. 6). Moreover, the PDGFB identified in HASC-CM could further stimulate the expression of MRTF-A-SRF-modulated genes in fibroblasts, as evidenced in developmental studies of cell migration (Vasudevan and Soriano, 2014).

In addition to the observed stimulation of EMT markers in HUFs, our results showed that HASC-CM treatment increases the amount of αSMA both in untreated and TGFβ-treated cells. We measured that the HASC-CM-stimulated expression of *ACTA2* in HUFs occurs at 3 and 12 h after stimulation, suggesting several stimulation events. Such increase in αSMA amount has also been observed in HASC-CM treated dermal fibroblasts (El-Hattab et al., 2020). Moreover, the treatment of the cells with a combination of HASC-CM and TGFβ significantly increased the expression of *COL1A1*, which is another marker for fibrosis progression. These results are similar to those gathered in another study investigating the effects of HASC-CM on fibroblasts (Yuan et al., 2017), however, it has been noted that the pro- or antifibrotic effect in that case depended on the dilution of HASC-CM, meaning, the concentration of molecules secreted by HASC into the medium. The suppression of SMAD5 signalling has been linked to transformation of bronchial fibroblasts into myofibroblasts, supporting our findings (Lin et al., 2024). Meanwhile, no such alterations were observed in our experiments conducted on WPMY-1 cells. Drawing on the conclusions from other studies (Walker et al., 2021; Kato et al., 2020), we can speculate that the WPMY-1 cells, derived from cancer tissue, present a different gene expression profile due to epigenetic changes, leading to altered interleukin or growth factor receptor levels. Thus, they may exhibit no changes after HASC-CM treatment.

Some studies employing *in vitro* fibrosis models have noted the anti-fibrotic activity of ASC-derived exosomes or ASCs themselves (Wang et al., 2024), however, these studies investigated the effects on fibroblasts cultivated on tissue culture plastic (Li et al., 2022; Wu et al., 2021). As both fibroblasts and myofibroblasts are mechanically sensitive cells, it is crucial to tune their culture surface elasticity to that of natural scar tissue, which has an elastic modulus of ~50 kPa (Davidson et al., 2020; Verma et al., 2023) and not the 2 GPa of plastic (Guimarães et al., 2020). In our study, the HUFs and WPMY-1 cells were cultured on fibronectin-coated PDMS with similar elasticity (Darby et al., 2022; Megone et al., 2018), which could explain some of the differences between the effects of HASC-CM on fibroblasts that we observed and those obtained by other researchers. The effect of matrix stiffness on the appearance of myofibroblast markers has been demonstrated in other studies, such as those investigating lung fibroblasts (Huang et al., 2012). In general, it is well established that the conditioned medium of ASCs and other mesenchymal stem cells has an anti-fibrotic effect *in vivo (*Choi et al., 2024a*)*, which could be at least partially explained by the immunomodulatory activity of these substances, as the suppression of inflammation at the site of tissue damage could prevent the activation of myofibroblasts.

Taken together, our data suggest that HASC-CM elicits pro-EMT changes in HUFs by suppressing SMAD5 phosphorylation, stimulating the subsequent nuclear translocation of MRTF-A and modulating gene expression through this factor, in combination with phospho-SMAD3 and/or SRF. The observed changes in gene expression and protein marker levels can be considered pro-fibrotic *in vitro*, as the cells transform into a myofibroblast phenotype. Interestingly, the combined treatment of HASC-CM and TGFβ attenuated SMAD5

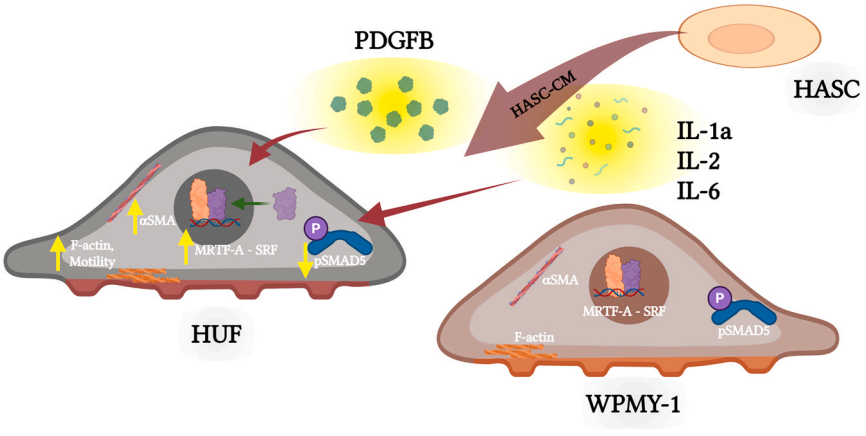

Fig. 6. Summary of identified active HASC-CM components and their effects on HUF cells, and the absence of effect on WPMY-1 cells.

dephosphorylation, suggesting that the effect of HASC-CM is dependent on the strength of TGFβ-activated signalling. In the context of therapeutic applications, our findings suggest that the whole HASC secretome, which constitutes the main component of HASC-CM, may have limited anti-fibrotic potential, although additional validation, especially in vivo, is needed. This does not exclude the possibility the isolated components of the HASC-CM, or those produced by genetically modified HASCs, would have a more positive therapeutic potential, as other studies have suggested (Filidou et al., 2022). Elucidating the precise mechanisms of action could be performed after the purification of molecules secreted by the HASCs into the medium and characterization of all the components of HASC-CM that originate from HASCs. This would facilitate focusing on the specific ligand-receptor interactions on the fibroblast membrane and the role of miRNAs in the processes we observed. Further analysis should be performed to establish the precise mechanism of the observed HASC-CM-stimulated dephosphorylation of SMAD5, and whether this inhibition of SMAD5 signaling could be controlled in a therapeutic setting.

5. Conclusions

The partial characterization of HASC-CM contents revealed the presence of PDGFB and the pro-inflammatory cytokines IL-1a, IL-2 and IL-6. HASC-CM induces the expression of mesenchymal and myofibroblast markers in primary human urethral fibroblasts, but not WPMY-1 cells. HASC-CM induced SMAD5 dephosphorylation, F-actin polymerization and MRTF-A nuclear translocation in human urethral fibroblasts, while also stimulating their motility. This resulted in the transcription of EMT-related genes *SNAIL1* and *SNAIL2*. Finally, HASC-CM stimulated the appearance of αSMA in human urethral fibroblasts, suggesting a pro-fibrotic effect. We did not detect these changes in WPMY-1 cells.

CRediT authorship contribution statement

Ieva Simoliune: Writing – review & editing, Methodology, Investigation, Formal analysis. **Daiva Baltriukiene:** Writing – review & editing, Supervision, Project administration, Conceptualization. **Aivaras Grybas:** Writing – review & editing, Methodology, Investigation. **Emilija Baltrukonyte:** Methodology, Investigation. **Povilas Barasa:** Writing – review & editing, Writing – original draft, Methodology, Investigation, Formal analysis, Conceptualization.

Declaration of Competing Interest

The authors declare that they have no known competing financial interests or personal relationships that could have appeared to influence the work reported in this paper.

Funding Information

This project received funding from the European Regional Development Fund (project no. 01.2.2-LMT-K-718-03-0087) under a grant agreement with the Research Council of Lithuania (LMTLT).

Appendix A. Supporting information

Supplementary data associated with this article can be found in the online version at doi:10.1016/j.ejcb.2026.151538.

Data availability

Data will be made available on request.

References

Allaire J.M., Darsigny M., Marcoux S.S., B Roy S.A., Schmouth J.F., Umans L., et al. Loss of Smad5 leads to the disassembly of the apical junctional complex and increased susceptibility to experimental colitis [Internet]. 2011. doi:10.1152/ajpgi.00041.2010.-The.

Bacakova, L., Zarubova, J., Travnickova, M., Musilkova, J., Pajorova, J., Slepicka, P., et al., 2018. Stem cells: their source, potency and use in regenerative therapies with focus on adipose-derived stem cells – a review. Jul 1 Biotechnol. Adv. 36 (4), 1111–1126. https://doi.org/10.1016/j.biotechadv.2018.03.011.

Baranyi U., Winter B., Gugerell A., Hegedus B., Brostjan C., Laufer G., et al. Primary Human Fibroblasts in Culture Switch to a Myofibroblast-Like Phenotype Independently of TGF Beta.(n.d).

Bari, E., Ferrarotti, I., Saracino, L., Perteghella, S., Torre, M.L., Richeldi, L., et al., 2021. Mesenchymal stromal cell secretome for post-covid-19 pulmonary fibrosis: a new therapy to treat the long-term lung sequelae? May 1 Cells 10 (5). https://doi.org/10.3390/cells10051203.

Basalova, N., Sagaradze, G., Arbatskiy, M., Evtushenko, E., Kulebyakin, K., Grigorieva, O., et al., 2020. Secretome of mesenchymal stromal cells prevents myofibroblasts differentiation by transferring fibrosis-associated microRNAs within extracellular vesicles. May 20 Cells 9 (5). https://doi.org/10.3390/cells9051272.

Bhattacharya, M., Ramachandran, P., 2023. Immunology of human fibrosis (Sep). Nat. Immunol. 24 (9), 1423–1433. https://doi.org/10.1038/s41590-023-01551-9.

Borthwick, L.A., 2016. The IL-1 cytokine family and its role in inflammation and fibrosis in the lung (Jul). Semin Immunopathol. 38 (4), 517–534. https://doi.org/10.1007/s00281-016-0559-z.

Chen, C.Y., Yang, S.H., Chang, P.Y., Chen, S.F., Nieh, S., Huang, W.Y., et al., 2024. Cancer-Associated-Fibroblast-Mediated Paracrine and Autocrine SDF-1/CXCR4 Signaling Promotes Stemness and Aggressiveness of Colorectal Cancers. Aug 12 Cells 13 (16), 1334. https://doi.org/10.3390/cells13161334.

Choi, Y.J., Kim, W.R., Kim, D.H., Kim, J.H., Yoo, J.H., 2024a. Human umbilical cord/placenta mesenchymal stem cell conditioned medium attenuates intestinal fibrosis in vivo and in vitro. Dec 1 Stem Cell Res Ther. 15 (1). https://doi.org/10.1186/s13287-024-03678-4.

Choi, Y.J., Kim, J.H., Lee, Y., Pyeon, H.J., Yoo, I.K., Yoo, J.H., 2024b. Anti-fibrogenic effect of umbilical cord–derived mesenchymal stem cell–conditioned media in human esophageal fibroblasts. Sep 27 Sci. Rep. 14 (1), 22233. https://doi.org/10.1038/s41598-024-73091-7.

Chung, J.Y.F., Chan, M.K.K., Li, J.S.F., Chan, A.S.W., Tang, P.C.T., Leung, K.T., et al., 2021. Tgf-β signaling: From tissue fibrosis to tumor microenvironment. Int J. Mol. Sci. 22 (14), 1–18. https://doi.org/10.3390/ijms22147575.

Curado, F., Spuul, P., Egaña, I., Rottiers, P., Daubon, T., Veillat, V., et al., 2014. ALK5 and ALK1 Play Antagonistic Roles in Transforming Growth Factor β-Induced Podosome Formation in Aortic Endothelial Cells. Dec 1 Mol. Cell Biol. 34 (24), 4389–4403. https://doi.org/10.1128/mcb.01026-14.

Darby, D.R., Cai, Z., Mason, C.R., Pham, J.T., 2022. Modulus and adhesion of Sylgard 184, Solaris, and Ecoflex 00-30 silicone elastomers with varied mixing ratios. Jul 5 J. Appl. Polym. Sci. 139 (25), e52412. https://doi.org/10.1002/app.52412.

Darby, I.A., Laverdet, B., Bonté, F., Desmoulière, A., 2014. Fibroblasts and myofibroblasts in wound healing. Clin. Cosmet. Invest. Dermatol. 7, 301–311. https://doi.org/10.2147/CCID.S50046.

Davidson, M.D., Burdick, J.A., Wells, R.G., 2020. Engineered Biomaterial Platforms to Study Fibrosis. Apr 1 Adv. Health Mater. 9 (8). https://doi.org/10.1002/adhm.201901682.

Distler, J.H.W., Györfi, A.H., Ramanujam, M., Whitfield, M.L., Königshoff, M., Lafyatis, R., 2019. Shared and distinct mechanisms of fibrosis (Dec). Nat. Rev. Rheuma 15 (12), 705–730. https://doi.org/10.1038/s41584-019-0322-7.

Du, P., Tao, X., Liu, K., Lin, J., Shi, Y., Park, K., et al., 2022. Human platelet lysate (hPL) alters the lineage commitment and paracrine functions of human mesenchymal stem cells via mitochondrial metabolism (Mar). Appl. Mater. Today 26, 101264. https://doi.org/10.1016/j.apmt.2021.101264.

El-Hattab, M.Y., Nagumo, Y., Gourronc, F.A., Klingelhutz, A.J., Ankrum, J.A., Sander, E. A., 2020. Human Adipocyte Conditioned Medium Promotes In Vitro Fibroblast Conversion to Myofibroblasts. Dec 1 Sci. Rep. 10 (1). https://doi.org/10.1038/s41598-020-67175-3.

Fabregat, I., Malfettone, A., Soukupova, J., 2016. New Insights into the Crossroads between EMT and Stemness in the Context of Cancer. Mar 12 J. Clin. Med 5 (3), 37. https://doi.org/10.3390/jcm5030037.

Feng, Y.L., Chen, D.Q., Vaziri, N.D., Guo, Y., Zhao, Y.Y., 2020. Small molecule inhibitors of epithelial-mesenchymal transition for the treatment of cancer and fibrosis. Med Res Rev. 40 (1), 54–78. https://doi.org/10.1002/med.21596.

Filidou, E., Kandilogiannakis, L., Tarapatzi, G., Spathakis, M., Steiropoulos, P., Mikroulis, D., et al., 2022. Anti-Inflammatory and Anti-Fibrotic Effect of Immortalized Mesenchymal-Stem-Cell-Derived Conditioned Medium on Human Lung Myofibroblasts and Epithelial Cells. Apr 20 Int J. Mol. Sci. 23 (9), 4570. https://doi.org/10.3390/ijms23094570.

Finnson, K.W., Almadani, Y., Philip, A., 2020. Non-canonical (non-SMAD2/3) TGF-β signaling in fibrosis: Mechanisms and targets. Semin Cell Dev. Biol. 101 (ember 2019), 115–122. https://doi.org/10.1016/j.semcdb.2019.11.013.

Francis Stuart, S.D., De Jesus, N.M., Lindsey, M.L., Ripplinger, C.M., 2016. The crossroads of inflammation, fibrosis, and arrhythmia following myocardial infarction. J. Mol. Cell Cardiol. 91, 114–122. https://doi.org/10.1016/j.yjmcc.2015.12.024.

Galie, P.A., Westfall, M.V., Stegemann, J.P., 2011. Reduced serum content and increased matrix stiffness promote the cardiac myofibroblast transition in 3D collagen matrices. Cardiovasc Pathol. 20 (6), 325–333. https://doi.org/10.1016/j.carpath.2010.10.001.

García-Palmero, I., Torres, S., Bartolomé, R.A., Peláez-García, A., Larriba, M.J., Lopez-Lucendo, M., et al., 2016. Twist1-induced activation of human fibroblasts promotes matrix stiffness by upregulating palladin and collagen α1(VI). Oct 6 Oncogene 35 (40), 5224–5236. https://doi.org/10.1038/onc.2016.57.

Garufi, A., Pistritto, G., D'Orazi, G., 2023. HIPK2 as a Novel Regulator of Fibrosis. Feb 7 Cancers 15 (4), 1059. https://doi.org/10.3390/cancers15041059.
Gau, D., Roy, P., 2018. SRF'ing and SAP'ing - The role of MRTF proteins in cell migration. Oct 1 J. Cell Sci. 131 (19). https://doi.org/10.1242/jcs.218222.
Ghosh, A.K., Vaughan, D.E., 2012. PAI-1 in tissue fibrosis. J. Cell Physiol. 227 (2), 493–507. https://doi.org/10.1002/jcp.22783.
Guimarães, C.F., Gasperini, L., Marques, A.P., Reis, R.L., 2020. The stiffness of living tissues and its implications for tissue engineering. May 1 Nat. Rev. Mater. 5 (5), 351–370. https://doi.org/10.1038/s41578-019-0169-1.
Harrell, C.R., Fellabaum, C., Jovicic, N., Djonov, V., Arsenijevic, N., Volarevic, V., 2019. Molecular mechanisms responsible for therapeutic potential of mesenchymal stem cell-derived secretome. May 1 Cells 8 (5). https://doi.org/10.3390/cells8050467.
Hillary, C.J., Osman, N.I., Chapple, C.R., 2014. Current trends in urethral stricture management (Oct). Asian J. Urol. 1 (1), 46–54. https://doi.org/10.1016/j.ajur.2015.04.005.
Hinz, B., 2015b. The extracellular matrix and transforming growth factor-β1: Tale of a strained relationship. Matrix Biol. 47, 54–65. https://doi.org/10.1016/j.matbio.2015.05.006.
Hinz, B., 2015a. Myofibroblasts. May 14 Exp. Eye Res 142, 56–70. https://doi.org/10.1016/j.exer.2015.07.009.
Hirano, Y., Horiguchi, A., Ojima, K., Azuma, R., Shinchi, M., Ito, K., et al., 2023. Myofibroblast-dominant proliferation associated with severe fibrosis in abulbar urethral strictures (Jan). Int J. Urol. 30 (1), 107–112. https://doi.org/10.1111/iju.15053.
Huang, M. jie, Ji, Y. wei, Chen, J. wen, Li, D., Zhou, T., Qi, P., et al., 2023. Targeted VEGFA therapy in regulating early acute kidney injury and late fibrosis (Sep). Acta Pharm. Sin. 44 (9), 1815–1825. https://doi.org/10.1038/s41401-023-01070-1.
Huang, X., Yang, N., Fiore, V.F., Barker, T.H., Sun, Y., Morris, S.W., et al., 2012. Matrix Stiffness–Induced Myofibroblast Differentiation Is Mediated by Intrinsic Mechanotransduction. Sep 1 Am. J. Respir. Cell Mol. Biol. 47 (3), 340–348. https://doi.org/10.1165/rcmb.2012-0050OC.
Iser, I.C., Ceschini, S.M., Onzi, G.R., Bertoni, A.P.S., Lenz, G., Wink, M.R., 2016. Conditioned Medium from Adipose-Derived Stem Cells (ADSCs) Promotes Epithelial-to-Mesenchymal-Like Transition (EMT-Like) in Glioma Cells In vitro. Dec 1 Mol. Neurobiol. 53 (10), 7184–7199. https://doi.org/10.1007/s12035-015-9585-4.
Kato, K., Logsdon, N.J., Shin, Y.J., Palumbo, S., Knox, A., Irish, J.D., et al., 2020. Impaired Myofibroblast Dedifferentiation Contributes to Nonresolving Fibrosis in Aging (May). Am. J. Respir. Cell Mol. Biol. 62 (5), 633–644. https://doi.org/10.1165/rcmb.2019-0092OC.
Kehl, D., Generali, M., Mallone, A., Heller, M., Uldry, A.C., Cheng, P., et al., 2019. Proteomic analysis of human mesenchymal stromal cell secretomes: a systematic comparison of the angiogenic potential. Apr 16 Npj Regen. Med 4 (1). https://doi.org/10.1038/s41536-019-0070-y.
Knuppel, L., Ishikawa, Y., Aichler, M., Heinzelmann, K., Hatz, R., Behr, J., et al., 2017. A novel antifibrotic mechanism of nintedanib and pirfenidone inhibition of collagen fibril assembly. Am. J. Respir. Cell Mol. Biol. 57 (1), 77–90. https://doi.org/10.1165/rcmb.2016-0217OC.
Kokabu, S., Katagiri, T., Yoda, T., Rosen, V., 2012. Role of Smad phosphatases in BMP-Smad signaling axis-induced osteoblast differentiation (May). J. Oral. Biosci. 54 (2), 73–78. https://doi.org/10.1016/j.job.2012.02.003.
Kruger, M.J., Conradie, M.M., Conradie, M., Van De Vyver, M., 2018. ADSC-conditioned media elicit an ex vivo anti-inflammatory macrophage response (Nov). J. Mol. Endocrinol. 61 (4), 173–184. https://doi.org/10.1530/JME-18-0078.
Latha, K.C., Sreekumar, A., Beena, V., Binil, R.S.S., Lakkappa, R.B., Kalyani, R., et al., 2021. Shear stress alterations activate BMP4/pSMAD5 signaling and induce endothelial mesenchymal transition in varicose veins. Dec 1 Cells 10 (12). https://doi.org/10.3390/cells10123563.
Lee, M.H., Kundu, J.K., Chae, J.I., Shim, J.H., 2019. Targeting ROCK/LIMK/cofilin signaling pathway in cancer. Jun 1 Arch. Pharm. Res 42 (6), 481–491. https://doi.org/10.1007/s12272-019-01153-w.
Lee, D.Y., Lee, S.Y., Yun, S.H., Jeong, J.W., Kim, J.H., Kim, H.W., et al., 2022. Review of the Current Research on Fetal Bovine Serum and the Development of Cultured Meat (Sep). Food Sci. Anim. Resour. 42 (5), 775–799. https://doi.org/10.5851/kosfa.2022.e46.
Lehrich, B.M., Liang, Y., Fiandaca, M.S., 2021. Foetal bovine serum influence on in vitro extracellular vesicle analyses (Jan). J. Extra Vesicles 10 (3). https://doi.org/10.1002/jev2.12061.
Lehtonen, S.T., Veijola, A., Karvonen, H., Lappi-Blanco, E., Sormunen, R., Korpela, S., et al., 2016. Pirfenidone and nintedanib modulate properties of fibroblasts and myofibroblasts in idiopathic pulmonary fibrosis. Respir. Res 17 (1), 1–12. https://doi.org/10.1186/s12931-016-0328-5.
Li, J., Li, Z., Wang, S., Bi, J., Huo, R., 2022. Exosomes from human adipose-derived mesenchymal stem cells inhibit production of extracellular matrix in keloid fibroblasts via downregulating transforming growth factor-β2 and Notch-1 expression. Apr 1 Bioengineered 13 (4), 8515–8525. https://doi.org/10.1080/21655979.2022.2051838.
Li, X., Luo, Q., Sun, J., Song, G., 2015. Conditioned medium from mesenchymal stem cells enhances the migration of hepatoma cells through CXCR4 up-regulation and F-actin remodeling. Mar 1 Biotechnol. Lett. 37 (3), 511–521. https://doi.org/10.1007/s10529-014-1710-3.
Li, L., Ngo, H.T.T., Hwang, E., Wei, X., Liu, Y., Liu, J., et al., 2019. Conditioned Medium from Human Adipose-Derived Mesenchymal Stem Cell Culture Prevents UVB-Induced Skin Aging in Human Keratinocytes and Dermal Fibroblasts. Dec 19 Int J. Mol. Sci. 21 (1), 49. https://doi.org/10.3390/ijms21010049.
Lin, Z., Zhuang, J., He, L., Zhu, S., Kong, W., Lu, W., et al., 2024. Exploring Smad5: a review to pave the way for a deeper understanding of the pathobiology of common respiratory diseases. Nov 22 Mol. Med 30 (1), 225. https://doi.org/10.1186/s10020-024-00961-1.
Lipson, K.E., Wong, C., Teng, Y., Spong, S., 2012. CTGF is a central mediator of tissue remodeling and fibrosis and its inhibition can reverse the process of fibrosis. Fibrogenes. Tissue Repair 5 (S1), 2–9. https://doi.org/10.1186/1755-1536-5-s1-s24.
Ma, H.Y., Vander Heiden, J.A., Uttarwar, S., Xi, Y., N'Diaye, E.N., LaCanna, R., et al., 2023. Inhibition of MRTF activation as a clinically achievable anti-fibrotic mechanism for pirfenidone. Apr 1 Eur. Respir. J. 61 (4). https://doi.org/10.1183/13993003.00604-2022.
Mangera, A., Chapple, C., 2010. Management of anterior urethral stricture: an evidence-based approach (Nov). Curr. Opin. Urol. 20 (6), 453–458. https://doi.org/10.1097/MOU.0b013e32833ee8d5.
Megone, W., Roohpour, N., Gautrot, J.E., 2018. Impact of surface adhesion and sample heterogeneity on the multiscale mechanical characterisation of soft biomaterials. Apr 30 Sci. Rep. 8 (1), 6780. https://doi.org/10.1038/s41598-018-24671-x.
Meng, X.M., Nikolic-Paterson, D.J., Lan, H.Y., 2016. TGF-β: The master regulator of fibrosis. Nat. Rev. Nephrol. 12 (6), 325–338. https://doi.org/10.1038/nrneph.2016.48.
Miranda, M.Z., Lichner, Z., Szászi, K., Kapus, A., 2021. Mrtf: Basic biology and role in kidney disease. Jun 1 Int J. Mol. Sci. 22 (11). https://doi.org/10.3390/ijms22116040.
Muñoz-Félix, J.M., González-Núñez, M., López-Novoa, J.M., 2013. ALK1-Smad1/5 signaling pathway in fibrosis development: Friend or foe? Cytokine Growth Factor Rev. 24 (6), 523–537. https://doi.org/10.1016/j.cytogfr.2013.08.002.
Nakamura, R., Nakajima, D., Sato, H., Endo, Y., Ohara, O., Kawashima, Y., 2021. A Simple Method for In-Depth Proteome Analysis of Mammalian Cell Culture Conditioned Media Containing Fetal Bovine Serum. Mar 4 Int J. Mol. Sci. 22 (5), 2565. https://doi.org/10.3390/ijms22052565.
Niada, S., Giannasi, C., Magagnotti, C., Andolfo, A., Brini, A.T., 2021. Proteomic analysis of extracellular vesicles and conditioned medium from human adipose-derived stem/stromal cells and dermal fibroblasts (Feb). J. Proteom. 232, 104069. https://doi.org/10.1016/j.jprot.2020.104069.
Oki, K., Yoshihara, S., Urushihata, M., Ghazizadeh, M., 2021. Anti-fibrotic effect of adipose-derived mesenchymal stem cell conditioned medium in muscle fibrosis. Eur. Rev. Med Pharm. Sci. 25.
Pang, M., Teng, Y., Huang, J., Yuan, Y., Lin, F., Xiong, C., 2017. Substrate stiffness promotes latent TGF-β1 activation in hepatocellular carcinoma. Jan 29 Biochem Biophys. Res Commun. 483 (1), 553–558. https://doi.org/10.1016/j.bbrc.2016.12.107.
Prihadi, J.C., Sugandi, S., Siregar, N.C., Soejono, G., Harahap, A., 2018. Imbalance in extracellular matrix degradation in urethral stricture. Res Rep. Urol. 10, 227–232. https://doi.org/10.2147/RRU.S178904.
Schaks, M., Giannone, G., Rottner, K., 2019. Actin dynamics in cell migration. Essays Biochem 63 (5), 483–495. https://doi.org/10.1042/EBC20190015.
Shin, J., Rhim, J., Kwon, Y., Choi, S.Y., Shin, S., Ha, C.W., et al., 2019. Comparative analysis of differentially secreted proteins in serum-free and serum-containing media by using BONCAT and pulsed SILAC. Dec 1 Sci. Rep. 9 (1). https://doi.org/10.1038/s41598-019-39650-z.
Sobierajska, K., Ciszewski, W.M., Macierzynska-Piotrowska, E., Klopocka, W., Przygodzka, P., Karakula, M., et al., 2020. The new model of snail expression regulation: The role of mrtfs in fast and slow endothelial–mesenchymal transition. Aug 2 Int J. Mol. Sci. 21 (16), 1–22. https://doi.org/10.3390/ijms21165875.
Trzyna, A., Banaś-Ząbczyk, A., 2021b. Adipose-derived stem cells secretome and its potential application in "stem cell-free therapy. Jun 13 Biomolecules 11 (6), 878. https://doi.org/10.3390/biom11060878.
Trzyna, A., Banaś-Ząbczyk, A., 2021a. Adipose-derived stem cells secretome and its potential application in "stem cell-free therapy. Jun 13 Biomolecules 11 (6), 878. https://doi.org/10.3390/biom11060878.
Usman, S., Waseem, N.H., Nguyen, T.K.N., Mohsin, S., Jamal, A., Teh, M.T., et al., 2021. Vimentin Is at the heart of epithelial mesenchymal transition (EMT) mediated metastasis. Oct 5 Cancers 13 (19), 4985. https://doi.org/10.3390/cancers13194985.
Vasudevan, H.N., Soriano, P., 2014. SRF regulates craniofacial development through selective recruitment of MRTF cofactors by PDGF signaling (Nov). Dev. Cell 31 (3), 332–344. https://doi.org/10.1016/j.devcel.2014.10.005.
Verma, B.K., Chatterjee, A., Kondaiah, P., Gundiah, N., 2023. Substrate stiffness modulates TGF-β activation and ECM-associated gene expression in fibroblasts. Aug 23 Bioengineering 10 (9), 998. https://doi.org/10.3390/bioengineering10090998.
Walker, C.J., Crocini, C., Ramirez, D., Killaars, A.R., Grim, J.C., Aguado, B.A., et al., 2021. Nuclear mechanosensing drives chromatin remodelling in persistently activated fibroblasts. Dec 1 Nat. Biomed. Eng. 5 (12), 1485–1499. https://doi.org/10.1038/s41551-021-00709-w.
Wang, M., Zhao, J., Li, J., Meng, M., Zhu, M., 2024. Insights into the role of adipose-derived stem cells and secretome: potential biology and clinical applications in hypertrophic scarring. May 12 Stem Cell Res Ther. 15 (1), 137. https://doi.org/10.1186/s13287-024-03749-6.
Webber, M.M., Trakul, N., Thraves, P.S., Bello-DeOcampo, D., Chu, W.W., Storto, P.D., et al., 1999. A human prostatic stromal myofibroblast cell line WPMY-1: A model for stromal-epithelial interactions in prostatic neoplasia. Carcinogenesis 20 (7), 1185–1192. https://doi.org/10.1093/carcin/20.7.1185.
Wu, Z.Y., Zhang, H.J., Zhou, Z.H., Li, Z.P., Liao, S.M., Wu, Z.Y., et al., 2021. The effect of inhibiting exosomes derived from adipose-derived stem cells via the TGF-β1/Smad

pathway on the fibrosis of keloid fibroblasts (Mar). Gland Surg. 10 (3), 1046–1056. https://doi.org/10.21037/gs-21-4.

Yano, F., Takeda, T., Kurokawa, T., Tsubaki, T., Chijimatsu, R., Inoue, K., et al., 2022. Effects of conditioned medium obtained from human adipose-derived stem cells on skin inflammation (Jun). Regen. Ther. 20, 72–77. https://doi.org/10.1016/j.reth.2022.03.009.

Yuan, B., Broadbent, J.A., Huan, J., Yang, H., 2017. The effects of adipose stem cell–conditioned media on fibrogenesis of dermal fibroblasts stimulated by transforming growth factor-β1. Apr;1 J. Burn Care Res. https://doi.org/10.1097/bcr.0000000000000558.